J. Micromech. Microeng. **19** (2009) 074004 (8pp) doi:10.1088/0960-1317/19/7/074004

A wide-bandwidth and high-sensitivity robust microgyroscope

Korhan Sahin[1], Emre Sahin[2], Said Emre Alper[3] and Tayfun Akin[2,3,4]

[1] Department of Mechanical Engineering, Carnegie Mellon University, Pittsburgh, PA 15213, USA
[2] Department of Electrical and Electronics Engineering, Middle East Technical University, Ankara, Turkey
[3] MEMS Research and Application Center, Middle East Technical University, Ankara, Turkey

E-mail: tayfun-akin@metu.edu.tr

Received 19 December 2008, in final form 26 March 2009
Published 30 June 2009
Online at stacks.iop.org/JMM/19/074004

Abstract
This paper reports a microgyroscope design concept with the help of a 2 degrees of freedom (DoF) sense mode to achieve a wide bandwidth without sacrificing mechanical and electronic sensitivity and to obtain robust operation against variations under ambient conditions. The design concept is demonstrated with a tuning fork microgyroscope fabricated with an in-house silicon-on-glass micromachining process. When the fabricated gyroscope is operated with a relatively wide bandwidth of 1 kHz, measurements show a relatively high raw mechanical sensitivity of 131 μV $(^\circ\ s^{-1})^{-1}$. The variation in the amplified mechanical sensitivity (scale factor) of the gyroscope is measured to be less than 0.38% for large ambient pressure variations such as from 40 to 500 mTorr. The bias instability and angle random walk of the gyroscope are measured to be 131° h^{-1} and 1.15° $h^{-1/2}$, respectively.

(Some figures in this article are in colour only in the electronic version)

1. Introduction

Three major challenges that face microgyroscope designs are mechanical sensitivity, operation bandwidth and robustness against environmental variations [1–3]. Theoretically, mechanical sensitivity is maximized by operating the gyroscope at vacuum and by matching the resonance frequencies of the drive and sense modes [2, 4]. However, a MEMS gyroscope designed for matched drive- and sense-mode frequencies at 10 kHz and having a sense-mode quality factor greater than 10 000 would theoretically have a bandwidth less than 1 Hz. Therefore, mode-matched structures can be considered for applications requiring very high sensitivity but significantly low bandwidth, limiting their use in most practical applications. Moreover, to keep the gyroscope operating under matched-mode conditions is challenging due to the instability of the resonance condition.

Another problem of matched-mode gyroscope operation is the dependence of the sensitivity to the mechanical quality factor of the sense mode, making the gyroscope highly susceptible to the variations under the ambient conditions. Mode matching also increases quadrature coupling, which degrades the stability and robustness of the gyroscope against environmental variations. There are microgyroscopes reported in the literature [5, 6] that have decoupled drive and sense modes with near-match resonance frequencies in order to improve the bandwidth and robustness against the performance of environmental variations. Still, the trade-off between the mechanical sensitivity and bandwidth requires a precise control of the relative mismatch between the drive and sense frequencies. Theoretically, a time-varying angular rotation rate with a frequency ω_{rotation} applied to the gyroscope will excite the sense-mode mechanical system at frequencies $\omega_{\text{drive}} \pm \omega_{\text{rotation}}$. A significant problem with matched-mode and near-matched-mode gyroscopes originates from this effect, such that the sense-mode mechanical oscillator will give different responses to applied time-varying angular rotation rates with the same amplitude but different frequencies. This effect limits the applicable amount of mode matching for gyroscope applications requiring reliable performance for both static and dynamic angular rate inputs.

The use of a closed-loop sense mode eliminates the need for precise control of mode frequencies by electronically

[4] Author to whom any correspondence should be addressed.

flattening the sharp resonance curve, allows a wide bandwidth operation due to this flattening effect and yields a robust operation against environmental variations [7]. However, the closed-loop sense-mode operation requires complicated force-feedback electronics, which degrades the signal-to-noise ratio of the closed-loop system compared to the open-loop sensing[5]. Moreover, assuring a stable closed-loop system may not be easy and may require advanced controller architectures [8].

Instead of using a closed-loop system, an open-loop system with an inherently robust mechanical gyroscope structure may take the advantage of using much simpler and low-noise electronics, while still achieving overall robustness comparable to that of closed-loop systems. There are approaches that partially preserve the advantages of closed-loop operation by improving either the mechanical sensitivity [9] or robustness against environmental variations [3, 10] of the closed-loop sense-mode operation by utilizing 2 degrees of freedom (DoF) sense-mode dynamic systems. By the use of a 2 DoF sense-mode dynamic system, the mechanical sensitivity of a gyroscope is improved by utilizing the dynamic amplification effect of the vibration amplitude of the sense mass with respect to the proof mass [9]. 2 DoF sense-mode dynamic systems are also utilized in order to improve the robustness of the gyroscope against environmental temperature variations by benefiting the very stable nonresonant operating conditions inherent in 2 DoF sense-mode dynamic systems [3, 10]. On the other hand, existing 2 DoF sense-mode gyroscopes do not simultaneously allow high sensitivity and wide bandwidth, i.e. increasing the bandwidth severely limits the maximum size of the mass on which the sensing comb fingers are attached, resulting in a significant reduction in the electronic sensitivity of the gyroscope. Therefore, there is the need for an improved mechanical structure that can preserve high sensitivity, wide bandwidth and robustness against environmental variation advantages of the closed-loop sense-mode operation without using complex feedback electronics.

This paper reports a new design concept for 2 DoF sense-mode dynamic systems that allows a wide operation bandwidth and high mechanical sensitivity without the need for precise frequency control and closed-loop feedback electronics. This design has been developed by independent research groups [11, 12] and deals with the limitations of the existing 2 DoF sense-mode gyroscope architecture on mechanical sensitivity, electronic sensitivity and operation frequency. The new design preserves the robustness against the performance of environmental variations of existing 2 DoF sense-mode gyroscopes while providing small bias instability and angle random walk due to an improved mechanical structure.

2. The new design concept

Figure 1 displays the schematic view of a 2 DoF sense-mode dynamic system showing the proof mass, m_1, that is subject to the Coriolis force, F_c, and the sense mass, m_2, generating the second degree of freedom. Such a system is known as a dynamic vibration absorber (DVA) [13] as it allows mechanical amplification of the vibration amplitude of the sense mass with respect to the proof mass, while keeping the vibration amplitude of the proof mass at a minimum. For this 2 DoF dynamic system, there are two resonance peaks between which there is a flat gain region on the magnitude receptance frequency response function (FRF) of the sense mass [14]. In order to maximize the mechanical sensitivity at the flat band, the natural frequencies of the individual 1 DoF mechanical oscillators need to be designed equal to each other and k_2 needs to be selected much lower than k_1 [9, 11, 12, 15]. This requires m_2 to be very small, limiting the number of capacitive sense fingers that can be attached to it, therefore limiting the electronic sensitivity of the gyroscope. Moreover, the spacing between the resonance peaks increases as the operating frequency of the gyroscope is increased, yielding reduction in mechanical sensitivity at the flat gain region [12, 15]. Hence, there is a limitation on the operating frequency of DVA-type 2 DoF sense-mode gyroscopes. Therefore, the DVA-type design offers very stable and high bandwidth operation at the cost of reduced mechanical sensitivity, reduced electronic sensitivity and limitations on the operating frequency.

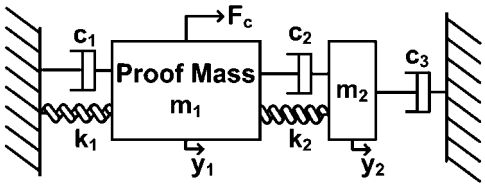

Figure 1. Schematic view of a DVA-type 2 DoF sense-mode dynamic system.

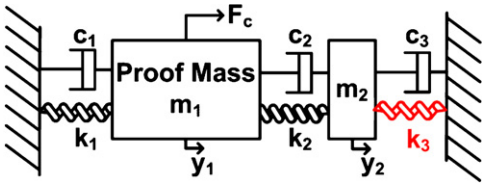

Figure 2. Schematic view of the proposed 2 DoF sense-mode dynamic system.

Figure 2 illustrates the schematic view of the proposed design that overcomes the limitations of the DVA-type sense-mode dynamic system design by including an additional spring k_3. Equation (1) demonstrates the dynamics of the proposed 2 DoF dynamic system in a matrix form [16]. In practical gyroscope applications, damping introduced into the system is minimized by the use of high quality structural materials such as single crystal silicon and by operating the gyroscope in vacuum environment. The resonance frequencies of an oscillatory mechanical system will be very close to the natural frequencies for small damping conditions; therefore (2), where $\omega_{m1} = \sqrt{\frac{k_1+k_2}{m_1}}$, $\omega_{m2} = \sqrt{\frac{k_2+k_3}{m_2}}$, $\alpha = \frac{k_2}{m_1}$ and $\beta = \frac{k_2}{m_2}$, is a good starting point in a design study. ω_{m1} and ω_{m2} are the natural frequencies of individual 1 DoF mechanical resonators. In (2), the damping matrix is discarded and sinusoidal solutions for y_1 and y_2 are assumed:

[5] MEMS Short Course Notes, available at http://www.eecs.berkeley.edu/~boser/pdf/feedback.pdf.

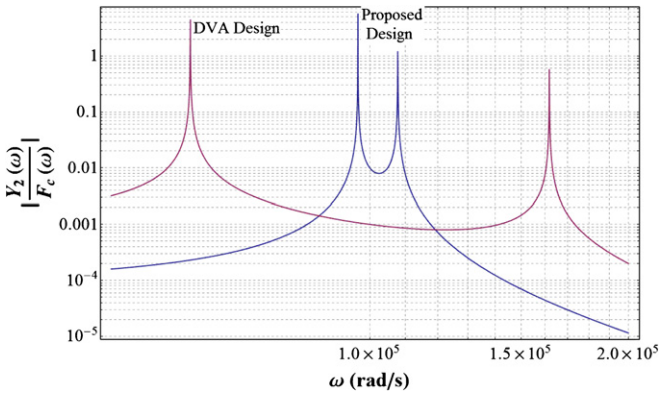

Figure 3. Magnitude receptance FRF plot showing that the mid-band mechanical sensitivity of the proposed design is much higher than that of a DVA-type design with the same sense mass.

$$\begin{bmatrix} m_1 & 0 \\ 0 & m_2 \end{bmatrix}\{\ddot{y}\} + \begin{bmatrix} c_1 + c_2 & -c_2 \\ -c_2 & (c_2 + c_3) \end{bmatrix}\{\dot{y}\} + \begin{bmatrix} k_1 + k_2 & -k_2 \\ -k_2 & k_2 + k_3 \end{bmatrix}\{y\} = \begin{Bmatrix} F_c \\ 0 \end{Bmatrix} \tag{1}$$

$$\begin{bmatrix} -\omega^2 + \omega_{m1}^2 & -\alpha \\ -\beta & -\omega^2 + \omega_{m2}^2 \end{bmatrix}\{Y(\omega)\} = \begin{Bmatrix} \dfrac{F_c}{m_1} \\ 0 \end{Bmatrix}. \tag{2}$$

Equations (3) and (4) demonstrate magnitude receptance FRFs of m_1 and m_2 for an undamped condition. For this dynamic system, the Coriolis force is applied to the proof mass in the presence of an applied angular rate input. The sense mass starts oscillations due to the coupling of the mechanical oscillations of the proof mass to the sense mass through k_2. Maximizing the oscillation amplitude of the sense mass with respect to the proof mass in the presence of a forcing on the proof mass is a convenient design guideline, as it is the mechanical oscillation amplitude of the sense mass that is measured to extract applied angular rate information.

The frequency at which the oscillation amplitude of the sense mass with respect to the proof mass is maximized is called the antiresonance frequency of a 2 DoF dynamic system [13]. Equation (5) demonstrates that antiresonance occurs at $\omega = \omega_{m2}$ for the proposed dynamic system. Hence, the operating frequency of the gyroscope, which is also the drive-mode resonance frequency, needs to be designed to satisfy the $\omega_d = \omega_{m1} = \omega_{m2}$ condition. This requirement is the same for the DVA design; on the other hand, k_2 can be designed to be much lower than k_1 without decreasing the magnitude of the sense mass, with the help of k_3 for the proposed design. Therefore, the proposed design overcomes the electronic sensitivity limitation of the DVA-type 2 DoF sense-mode gyroscopes.

Figure 3 illustrates the magnitude receptance FRF plot showing that the mid-band mechanical sensitivity of the proposed design is much higher than that of a DVA-type design with the same sense mass. Moreover, the sense-mode resonant spacing can be kept at reasonable values even at high operating frequencies, thereby verifying the overcoming of the limitation on the operating frequency inherent in DVA-type sense-mode gyroscopes. It is clear from figure 3 that the improvement in the mechanical sensitivity of the proposed design is at the cost of a reduced bandwidth. On the other hand, the bandwidth value offered by the DVA-type design is unnecessarily high [1], which cannot be reduced further without sacrificing electronic sensitivity due to the very limited size of the required sense mass. The proposed 2 DoF design concept eliminates this limitation by offering flexible adjustment of the bandwidth without sacrificing the sense mass and hence the electronic sensitivity:

$$\left|\frac{Y_1(\omega)}{F_c(\omega)}\right| = \frac{-\omega^2 + \omega_{m2}^2}{m_1\left[\alpha\beta - \left(-\omega^2 + \omega_{m1}^2\right)\left(-\omega^2 + \omega_{m2}^2\right)\right]} \tag{3}$$

$$\left|\frac{Y_2(\omega)}{F_c(\omega)}\right| = \frac{\beta}{m_1\left[\alpha\beta - \left(-\omega^2 + \omega_{m1}^2\right)\left(-\omega^2 + \omega_{m2}^2\right)\right]} \tag{4}$$

$$\left|\frac{Y_2(\omega)}{Y_1(\omega)}\right| = \frac{\beta}{-\omega^2 + \omega_{m2}^2}. \tag{5}$$

Equation (6) demonstrates the natural frequencies ω_{n1} and ω_{n2} of the proposed 2 DoF dynamic system for $\omega_{m1} = \omega_{m2}$. Equation (7) demonstrates $\omega_{n2}^2 - \omega_{n1}^2$ where $\omega_{\text{mid}} = \frac{\omega_{n1}+\omega_{n2}}{2}$ and $\Delta = \omega_{n2} - \omega_{n1}$. ω_{mid} can be simplified as given in (8) using (6) and (7). From (8), ω_{mid} can be approximated as ω_{m2} for practical designs. Hence, the spacing between the resonant peaks of the proposed 2 DoF dynamic system design will be approximately as given in (9). From (9) it can be concluded that, for constant proof mass and sense mass values, the resonant peak spacing can be adjusted independent of the operating frequency by varying the k_2 value while keeping $k_2 + k_3$ and $k_1 + \text{k}_2$ values constant. Hence, (9) theoretically verifies the overcoming of the limitation of the DVA-type design on the operating frequency:

$$\omega_{n1,n2} = \sqrt{\omega_{m2}^2 \pm \sqrt{\alpha\beta}} \tag{6}$$

$$\omega_{n2}^2 - \omega_{n1}^2 = 2\Delta\omega_{\text{mid}} = 2\sqrt{\alpha\beta} \tag{7}$$

$$\omega_{\text{mid}} = \frac{\omega_{m2}^2 + \sqrt{\omega_{m2}^4 - \alpha\beta}}{2} \cong \omega_{m2} \tag{8}$$

$$\Delta \cong \frac{\sqrt{\alpha\beta}}{\omega_{m2}} = \frac{k_2}{\sqrt{m_1(k_2 + k_3)}}. \tag{9}$$

Figure 4 demonstrates the magnitude receptance FRF plots for two gyroscopes with mechanical design parameters given in table 1 so that the proposed design can be compared with a matched-mode gyroscope. The design parameters are chosen according to [17], which states that a matched-mode gyroscope employing quality factors >30 000, proof mass >100 μg and drive-mode oscillation amplitude >5 μm is required in order to achieve inertial grade performance. It is observed from figure 4 that the mechanical sensitivity of the matched-mode design is much better than the proposed design due to the resonance effect at the operating frequency of a 1 DoF design. Therefore, a 1 DoF matched-mode design should be the choice for applications requiring high sensitivity where the operation bandwidth is not a concern. On the other hand, it is clear that as a mode mismatch is introduced to improve the bandwidth of the 1 DoF gyroscope, the mechanical

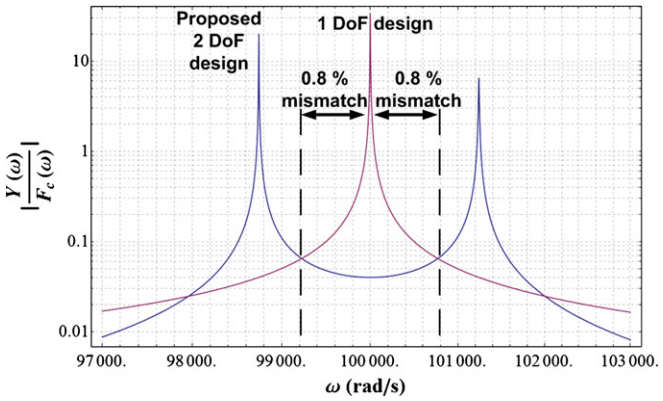

Figure 4. Magnitude receptance FRF plots of the sense mode of a 1 DoF matched-mode gyroscope and proposed 2 DoF sense-mode gyroscope.

Table 1. Mechanical design parameters of the 1 DoF matched-mode gyroscope and proposed 2 DoF sense-mode gyroscope.

1 DoF matched-mode design	Proposed 2 DoF design
$m = 100\ \mu$g	$m_1 = m_2 = 100\ \mu$g
	$k_1 = 975$ N m^{-1}
$k_d = k_s = 1000$ N m^{-1}	$k_2 = 25$ N m^{-1}
	$k_3 = 975$ N m^{-1}
$\omega_n = 100\,000$ rad s^{-1}	$\omega_{m1} = \omega_{m2} = 100\,000$ rad s^{-1}
$c_1 = c_2 = c_3 = 2.5 \times 10^{-7}$ Ns m^{-1}	$c_1 = c_2 = c_3 = 2.5 \times 10^{-7}$ Ns m^{-1}
Expected $Q = 40\,000$	Expected $Q = 40\,000$

sensitivity of the 1 DoF design degrades very rapidly and gets close to the proposed 2 DoF design.

For the representative example in figure 4, a mismatch of 0.8% introduced to the 1 DoF gyroscope will result in an amplitude response equivalent to the proposed 2 DoF sense-mode dynamic system. This 0.8% mismatch is equivalent to an open-loop sensor bandwidth of 128 Hz for the 1 DoF design. For inertial grade operation, the operation bandwidth should be around 100 Hz [1]; therefore, a near matched-mode design providing a sufficient bandwidth for inertial grade operation will be equivalent to the proposed 2 DoF gyroscope in terms of sensitivity. Hence, the proposed design concept has the potential to compete with its 1 DoF counterparts for applications requiring a high operation bandwidth and a high sensitivity simultaneously. More importantly, the proposed design has a sensitivity and bandwidth much more robust compared to the 1 DoF sensor concept, whose sensitivity and bandwidth are subject to change from their set values under varying ambient conditions such as pressure and temperature.

Figure 5 shows the schematic view of the designed multi-DoF tuning fork gyroscope utilizing the proposed sense-mode dynamic system. The drive frames and sense masses are restricted to 1 DoF motion along the x- and y-axes, respectively, providing mechanical decoupling between drive and sense modes. The proof masses have motion capability along both x- and y-axes. For this design, m_1 acts both as the proof mass and as a decoupling frame by the use of 2 DoF flexure structures. The gyroscope is designed to be in tuning fork configuration rejecting common-mode linear accelerations [8, 18].

3. Implementation and test results

The proposed gyroscope is fabricated using an in-house silicon-on-glass (SOG) micromachining process developed at METU MEMS cleanroom facilities [6]. Figure 6(*a*) shows the SEM picture of the fabricated gyroscope, while figure 6(*b*) is another SEM picture zoomed to the 2 DoF flexure structure that gives m_1 the ability to act both as the proof mass and as the decoupling frame. Capacitive signal coupling due to stray capacitances is a big problem in MEMS gyroscopes that causes stability problems in sustained oscillations of the drive mode and unwanted noise in the sense-mode output [19]. CMOS-MEMS-integrated gyroscopes have been developed to overcome the challenges due to capacitive coupling [20]. On the other hand, integrated gyroscopes have a limitation on the thermal-mechanical noise performance due to their limited proof mass values. Therefore, ways of integrating high proof mass surface micromachined and bulk micromachined gyroscopes with readout electronics on a hybrid package with the shortest possible distance is a good alternative to CMOS-MEMS gyroscopes. Figure 7 shows the photograph of the fabricated gyroscope, hybrid integrated with preamplifiers inside a platform package.

After the fabricated gyroscope is hybrid connected to preamplifiers, first the drive-mode frequency response characteristic is obtained to measure the operating frequency and the quality factor of the drive-mode resonator. Figure 8 shows the drive-mode frequency response measured at 20 V proof mass voltage (V_{PM}) and at 25 mTorr vacuum. The operating frequency of the gyroscope is measured to be 15 155 Hz with a quality factor of 8760. The negative electrostatic spring effect of varying-gap capacitive fingers needs to be considered while characterizing the sense-mode frequency response. Increasing V_{PM} decreases k_3 due to the negative electrostatic spring effect of varying-gap capacitive fingers, hence increasing the spacing between the resonant peaks as expected from (9).

Figure 9 shows the measured sense-mode frequency response curves for different V_{PM} voltages. It is clear from figure 9 that the negative electrostatic spring effect can be utilized to adjust the operation bandwidth. Next, the robustness of the proposed sense-mode dynamic system against environmental pressure variations under constant V_{PM} is examined. Figure 10 shows the measured frequency response of the sense mode at $V_{PM} = 35$ V for different vacuum ambient conditions. The sense-mode response around the operating frequency of the gyroscope (15 155 Hz) is almost constant for different vacuum levels verifying the robustness of the proposed design to ambient pressure variations. The flat band of figure 10 extends up to 2.5 kHz, which can be the maximum system bandwidth provided that the operating frequency of the gyroscope is set to 16.25 kHz. Next, the gyroscope is connected to external electronics providing closed-loop automatic gain control for the drive-mode vibrations and open−loop rate sensing.

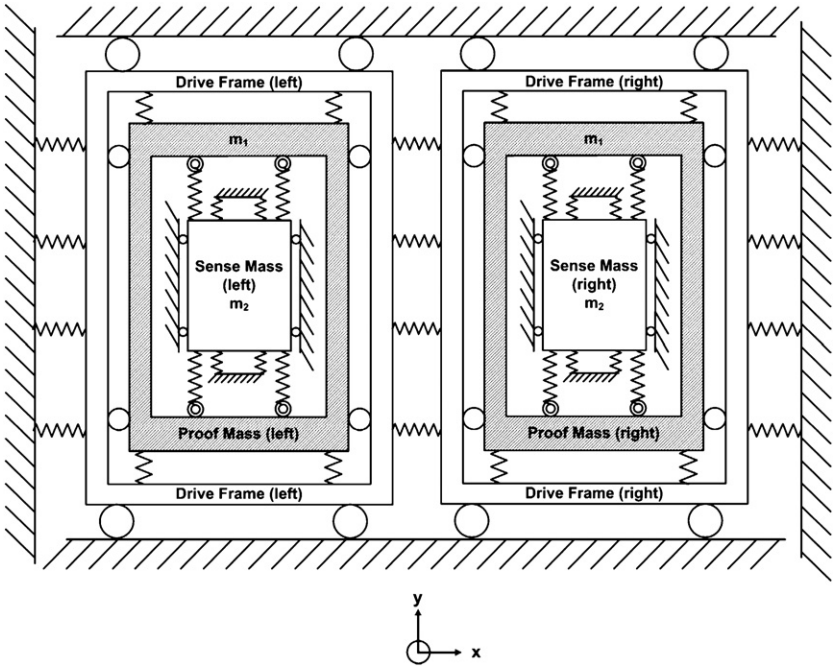

Figure 5. Schematic view of the designed multi-DoF tuning fork gyroscope.

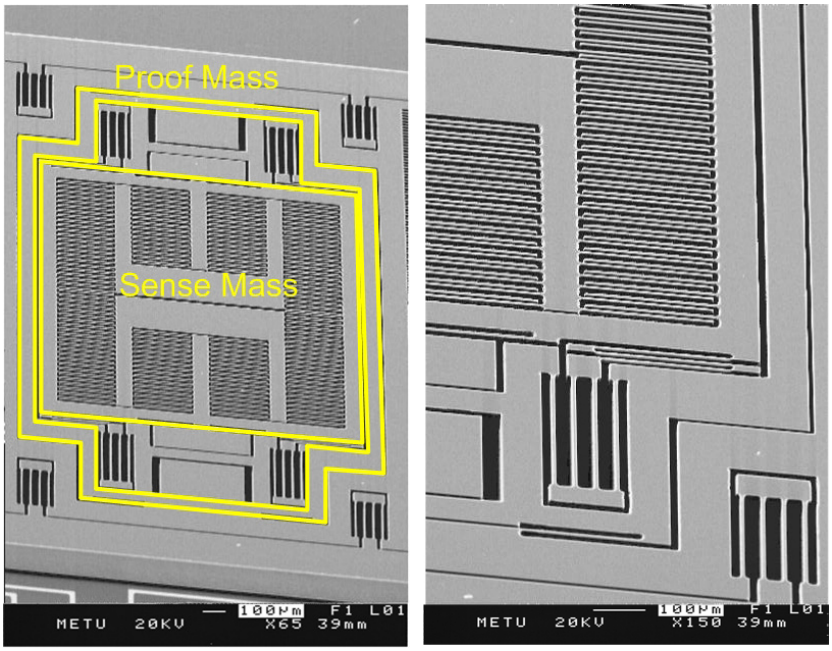

(*a*) (*b*)

Figure 6. (*a*) General SEM view of the fabricated gyroscope. (*b*) 2 DoF flexure structure that gives m_1 the ability to act both as the proof mass and as the decoupling frame.

Figure 11 shows the measured dc output of the gyroscope in response to constant angular rate inputs from the zero rate up to $\pm 100^\circ$ s^{-1} using 10° s^{-1} steps and then back to the zero rate, at 35 V proof mass voltage and 40 mTorr vacuum.

The time history at each step of the measured response to the constant angular rate inputs from -100° s^{-1} up to $+100^\circ$ s^{-1} is time averaged to determine the scale factor of the gyroscope. Figure 12 shows the measured scale factor and R^2 linearity of the output response of the gyroscope. The gyroscope demonstrates a scale factor of 13.1 mV $(^\circ \text{ s}^{-1})^{-1}$ in a measurement range of $\pm 100^\circ$ s^{-1}, with 40 dB amplification of the raw sense output. The R^2 parameter, which is the indicator of the deviation of the measured output response from a perfect linear fit, signifies the linearity of the measured scale factor to be better than 99.9% within a $\pm 100^\circ$ s^{-1} full scale.

Table 2 shows the measured scale factor and R^2 linearity values for different ambient pressures from 40 mTorr to 500 mTorr to verify the pressure robustness of the gyroscope

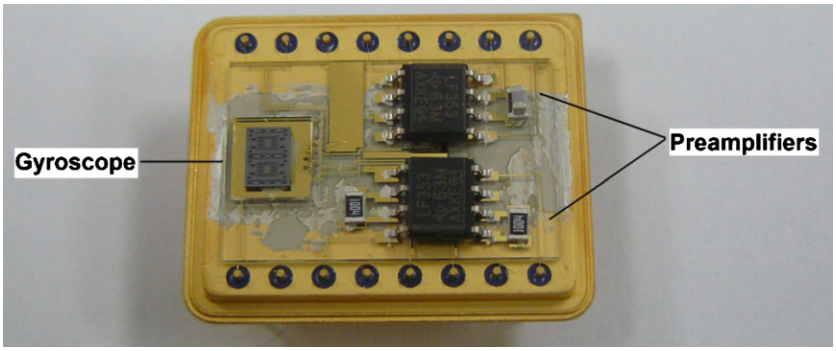

Figure 7. Photograph of the fabricated gyroscope, hybrid integrated with preamplifiers inside a platform package.

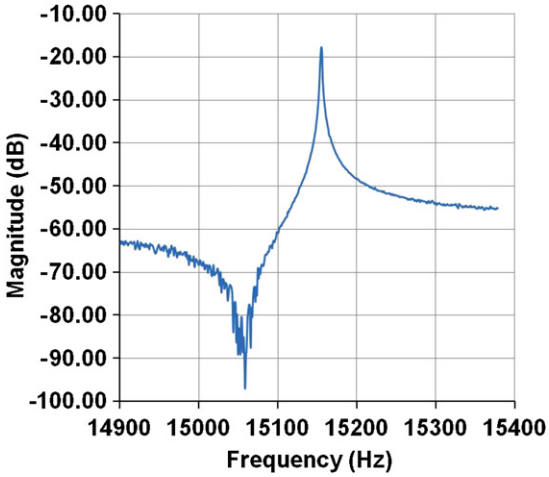

Figure 8. Drive-mode frequency response measured at 20 V proof mass voltage (V_{PM}) and at 25 mTorr vacuum.

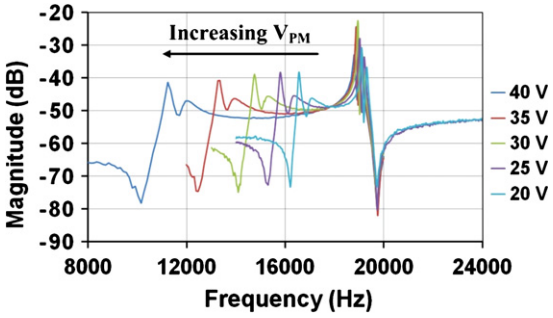

Figure 9. Measured sense-mode frequency response curves for different V_{PM} voltages.

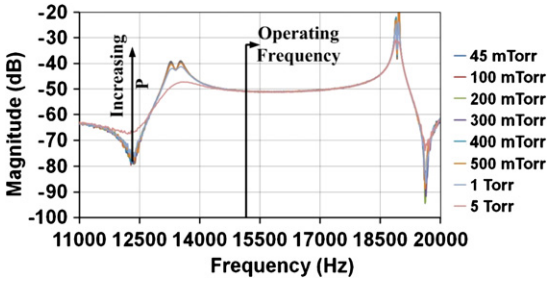

Figure 10. Measured frequency response of the sense mode at $V_{PM} = 35$ V for different vacuum ambient conditions.

output response, in addition to the pressure robustness of the proposed 2 DoF dynamic system. The variation in the scale

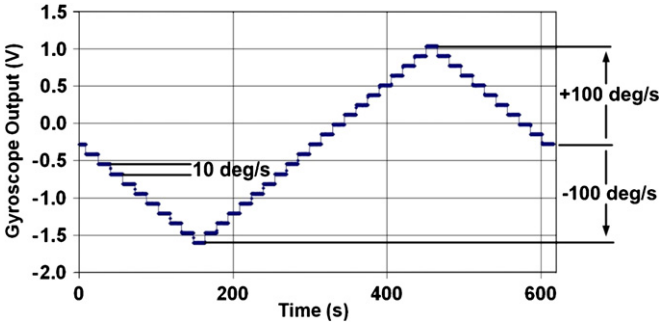

Figure 11. Measured dc output of the gyroscope in response to constant angular rate inputs from the zero rate up to $\pm 100^{\circ}$ s^{-1} using 10° s^{-1} steps and then back to the zero rate.

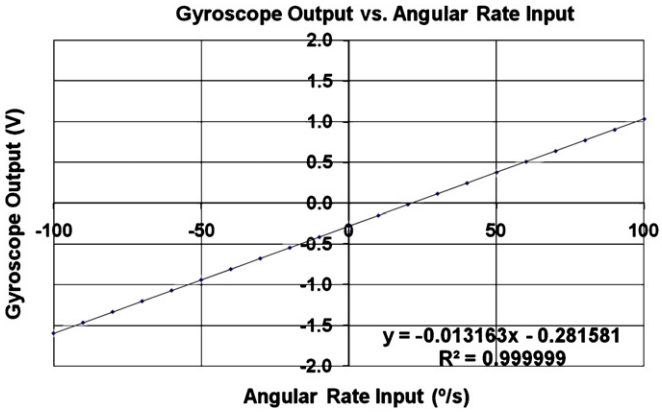

Figure 12. Measured scale factor and R^2 linearity of the output response of the gyroscope in a measurement range of $\pm 100^{\circ}$ s^{-1}.

factor of the gyroscope is measured to be less than 0.38%, proving the robustness of the gyroscope against ambient pressure variations. The verified pressure robustness of the proposed design concept and the fabricated gyroscope are promising for practical gyroscope applications that require complex vacuum-sealed packages to prevent leakage.

Figure 13 shows the output of the gyroscope in response to sinusoidal angular rate inputs with an amplitude of 1.25° s^{-1} and frequencies of 1, 2 and 4 Hz. These results show that the gyroscope provides an identical scale factor for angular rate inputs with different frequencies; however, this test could not be performed for frequencies over 4 Hz due to the limitations from the test equipment used for data acquisition. Data acquisition is performed by HPVEE software controlling an

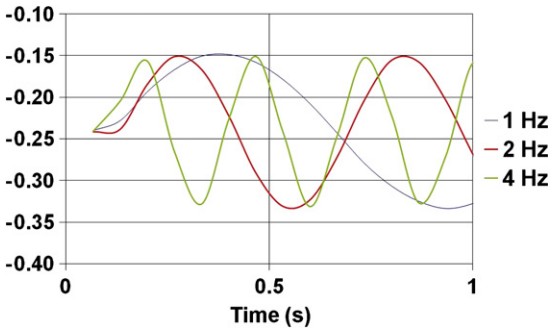

Figure 13. Output of the gyroscope in response to sinusoidal angular rate inputs with an amplitude of 1.25° s^{-1} and frequencies of 1, 2 and 4 Hz.

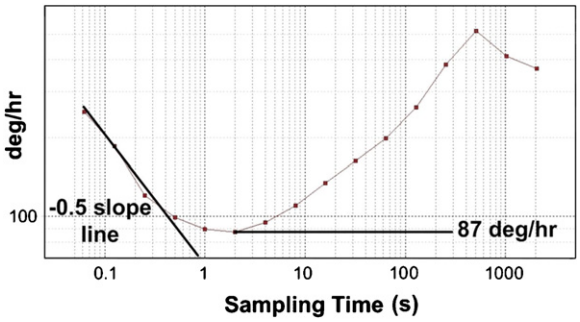

Figure 14. Allan variance plot of the measured long−term (2 h) zero rate output of the gyroscope.

Table 2. Scale factor and R^2 linearity for varying vacuum levels.

Pressure (mTorr)	Scale factor (mV (° s^{-1}) $^{-1}$)	R^2 Linearity (%)
40	−13.163	99.9999
100	−13.142	99.9999
200	−13.176	99.9999
300	−13.149	99.9999
400	−13.210	99.9998
500	−13.213	99.9994

Agilent multimeter, whose sampling rate is limited by 15 Hz. Therefore, the response of the gyroscope to sinusoidal angular rate inputs with frequencies greater than 4 Hz could not be sampled with a sufficient rate, even though the mechanical bandwidth of the sense-mode dynamic system is estimated from the measurement result presented in figure 10 to be about 1 kHz at 35 V proof mass voltage.

Gyroscope performance is also characterized using Allan variance analysis. The Allan variance analysis is a useful method to characterize the sources of random processes that result in unwanted noise observed in the gyroscope output [21]. Electronics susceptible to random flickering result in a noise at the output of the gyroscope that has a low-frequency nature, and this noise shows itself as bias fluctuations in the measured data. The square root Allan variance ($\sigma(\tau)$) value at the plateau of the Allan variance curve is 0.664 times the bias instability coefficient while the value of the −0.5 slope line fitted to the Allan variance curve at $\tau = 1$ s gives the angle random walk value. Figure 14 shows the Allan variance plot of the measured long-term (2 h) zero rate output of the gyroscope. The gyroscope demonstrates a bias instability and an angle random walk of 131° h^{-1} (87° h^{-1}/0.664) and 1.15° $h^{-1/2}$, respectively.

4. Conclusions

This study reports the realization of a new 2 DoF design concept providing a wide operation bandwidth and high mechanical gain to high−performance microgyroscopes that are robust against environmental variations. The proposed design has a bandwidth and robustness comparable to a DVA design, with an advantage of higher electronic sensitivity. Moreover, it provides a bandwidth and sensitivity comparable to a 1 DoF gyroscope with the near-matched-mode operation, while adding the advantage of higher robustness. Finally, it eliminates the need for complex feedback electronics implemented in closed-loop sensing by employing an inherently robust mechanical structure. The proposed concept is verified by the characterization of a tuning fork microgyroscope fabricated with an in-house silicon-on-glass micromachining process. The fabricated gyroscope is hybrid integrated with preamplifiers on a platform package to minimize the effects of capacitive coupling due to stray capacitances. The hybrid package connected to an external closed-loop drive-mode amplitude control and open-loop sense-mode readout electronics has shown a bias instability performance of 131° h^{-1} with an angle random walk value of 1.15° $h^{-1/2}$. The noise performance of the system is believed to be dominated by the simple readout and control circuitry, which can be improved by the selection of dedicated electronic components.

References

[1] Yazdi N, Ayazi F and Najafi K 1998 Micromachined inertial sensors *Proc. IEEE* **86** 1640–59
[2] Baek S S, Oh Y S, Ha B J, An S D, An B H, Song H and Song C M 1999 A symmetrical z-axis gyroscope with a high aspect ratio using simple and new process *12th IEEE Int. Conf. on Micro Electro Mechanical Systems (MEMS '99) (Jan. 1999)* pp 612–7
[3] Acar C and Shkel A M 2006 Inherently robust micromachined gyroscopes with 2-DOF sense-mode oscillator *IEEE/ASME J. Microelectromech. Syst.* **15** 380–7
[4] Sharma A, Zaman M F, Zucher M and Ayazi F 2008 A 0.1°/HR bias drift electronically matched tuning fork microgyroscope *21st IEEE Int. Conf. on Micro Electro Mechanical Systems (MEMS 2008) (6–9 Jan.)* pp 6–9
[5] Geiger W *et al* 2002 Decoupled microgyros and the design principle DAVED *Sensors Actuators* A **95** 239–49
[6] Alper S E, Temiz Y and Akin T 2008 A compact angular rate sensor system using a fully-decoupled silicon-on-glass MEMS gyroscope *IEEE/ASME J. Microelectromech. Syst.* **17** 1418–29
[7] Kranz M, Burgett S, Hudson T, Buncick M, Ruffin P, Ashley P and McKee J 2003 A wide dynamic range silicon-on-insulator MEMS gyroscope with digital force feedback *Transducers 2003* vol 1 159–62
[8] Boser B 1997 *RF Analog-to-Digital Converters; Sensor and Actuator Interfaces; Low-Noise Oscillators, PLLs and Synthesizers* ed R J van de Plassche, J H Huijsing and W M C Sansen (Dordrecht: Kluwer)

[9] Li X, Lin R and Leow K W 2000 Performance-enhanced micro-machined resonant systems with two-degrees-of-freedom resonators *J. Micromech. Microeng.* **10** 534–9
[10] Schofield A R, Trusov A A, Acar C and Shkel A M 2007 Anti-phase driven rate gyroscope with multi-degree of freedom sense mode *Transducers '07* 1199–202
[11] Sahin K, Sahin E, Alper S E and Akin T 2008 A wide-bandwidth and high-sensitivity robust microgyroscope *19th MicroMechanics Europe Workshop (MME 2008) (Aachen, Germany, 28–30 Sep.)* pp 97–100
[12] Trusov A A, Schofield A R and Shkel A M 2008 New architectural design of a temperature robust MEMS gyroscope with improved gain-bandwidth characteristics *Solid-State Sensors, Actuators, and Microsystems Workshop (Hilton Head, SC, 1–5 Jun.)* pp 14–7
[13] Dyck C W, Allen J and Hueber R 1999 Parallel plate electrostatic dual-mass oscillator *Proc. SPIE Conf. Micromachining Microfabrication* vol 3876 pp 198–209
[14] He J and Zhi F F 2001 *Modal Analysis* (Oxford, MA: Butterworth-Heinemann)
[15] Schofield A R, Trusov A A and Shkel A M 2008 Effects of operational frequency scaling in multi-degree of freedom MEMS gyroscopes *IEEE Sensors J.* **8** 1672–80
[16] Vierck R 1979 *Vibration Analysis* (New York: Harper and Row)
[17] Sharma A, Zaman F M, Amini B V and Ayazi F 2004 A high-Q in-plane SOI tuning fork gyroscope *proc. IEEE Sensors* vol 1 pp 467–70
[18] Bernstein J, Cho S, King A T, Kourepenis A, Maciel P and Weinberg M 1993 A micromachined comb-drive tuning fork rate gyroscope *MEMS '93* pp 143–8
[19] Alper S E, Sahin K and Akin T An analysis to improve stability of drive-mode oscillations in capacitive vibratory MEMS gyroscopes *22nd IEEE Int. Conf. on Micro Electro Mechanical Systems (MEMS 2009) (Italy, Jan. 2009)* pp 817–20
[20] Xie H and Fedder G K 2003 Integrated microelectromechanical gyroscopes *J. Aerospace Eng.* **16** 65–75
[21] IEEE Std 952-1997 1997 IEEE Standard Specification Format Guide and Test Procedure for Single-Axis Interferometric Fiber Optic Gyros